

Simultaneous Magnetic Manipulation and Fluorescent Tracking of Multiple Individual Hybrid Nanostructures

Gang Ruan,^{†,‡} Greg Vieira,^{§,†} Thomas Henighan,[§] Aaron Chen,[§] Dhananjay Thakur,^{||} R. Sooryakumar,^{*,§,†} and Jessica O. Winter^{*,†,||,⊥,‡}

[†]William G. Lowrie Department of Chemical and Biomolecular Engineering, [§]Department of Physics, ^{||}Biophysics Program, and [⊥]Department of Biomedical Engineering, The Ohio State University, Columbus, Ohio 43210

ABSTRACT Controlled transport of multiple individual nanostructures is crucial for nanoassembly and nanodelivery but is challenging because of small particle size. Although atomic force microscopy and optical and magnetic tweezers can control single particles, it is extremely difficult to scale these technologies for multiple structures. Here, we demonstrate a “nano-conveyer-belt” technology that permits simultaneous transport and tracking of multiple individual nanospecies in a selected direction. The technology consists of two components: nanocontainers, which encapsulate the nanomaterials transported, and nanoconveyer arrays, which use magnetic force to manipulate individual or aggregate nanocontainers. This technology is extremely versatile. For example, nanocontainers encapsulate quantum dots or rods and superparamagnetic iron oxide nanoparticles in <100 nm nanocontainers, the smallest magnetic composites to have been simultaneously moved and optically tracked. Similarly, the nanoconveyers consist of patterned microdisks or zigzag nanowires, whose dimensions can be controlled through micropatterning. The nanoconveyer belt technology could impact multiple fields, including nanoassembly, biomechanics, nanomedicine, and nanofluidics.

KEYWORDS Magnetic nanoparticle, quantum dot, self-assembly, magnetic tweezers, nanopatterning

The ability to simultaneously control multiple individual nanostructures is the cornerstone of bottom-up assembly strategies, with possible applications that range from video displays to therapeutics that can diagnose, treat, and monitor disease.^{1,2} The small size of nanostructures provides two significant challenges in controlled transport of multiple nanostructures: (1) separate large external fields may be required to manipulate each particle,^{3–5} and (2) it is difficult to track the motion of structures below 200 nm using traditional optical microscopy. Here, we describe a “nano-conveyer-belt” platform technology for simultaneous manipulation and optical tracking of multiple nanostructures. This technology is based on two key components. Polymeric micelle nanocontainers (~35 nm) encapsulating separate quantum dots (QDs) and iron oxide nanoparticles (i.e., hybrid magnetic quantum dots, HMQDs⁶) permit magnetic manipulation with simultaneous fluorescent observation, and patterned magnetic nanoconveyer arrays provide the tunable, high magnetic field gradients needed for controlled particle motion.^{7,8} This nano-conveyer-belt technology, which permits simultaneous observation and control of nanostructure movement, will

open new avenues in nanofabrication, nanofluidics, biomechanics, drug delivery, magnetic actuation, and molecular detection.

Two critical features in controlled motion of nanomaterials are providing a sufficient force for movement and a visualization scheme to track that motion. We have overcome these challenges with two enabling technologies: nanocontainers and nanoconveyers. Nanocontainers consist of polymeric micelles encapsulating HMQDs, which permit particle motion via magnetic fields and observation of that motion via fluorescence microscopy. Nanoconveyers are composed of patterned magnetic nanowires or disks with three orthogonal and addressable weak magnetic fields. Nanocontainer motion is controlled by nanoconveyers, which propagate containers along the length of the conveyer belt or enable, on-demand, capture and release of the containers in a flow stream (Figure 1).

Nanocontainers are composed of ~35 nm polymeric micelles with a hydrophobic core, into which hydrophobic nanostructures can be incorporated. To provide both manipulation and observation properties, we have encapsulated superparamagnetic iron oxide nanoparticles (SPIONs) and semiconductor quantum dots (QDs) within this core to yield HMQDs. Manipulation of magnetic micro- and nanoparticles containing iron oxide has been demonstrated with magnetic bead force application⁹ and magnetic tweezers techniques.¹⁰ However, in situ manipulation and tracking of single sub-100-nm magnetic nanoparticles has not yet been demonstrated, primarily because of difficulties in observing their

* To whom correspondence should be addressed: R. Sooryakumar, 191 West Woodruff Ave, Columbus, OH 43210, phone 614-292-3130, fax 614-292-7557, soory@mps.ohio-state.edu; Jessica O. Winter, 140 West 19th Ave, Columbus, OH 43210, phone 614-247-7668, fax 614-292-3769, winter.63@osu.edu.

† These authors contributed equally to this work.

Received for review: 04/5/2010

Published on Web: 05/07/2010



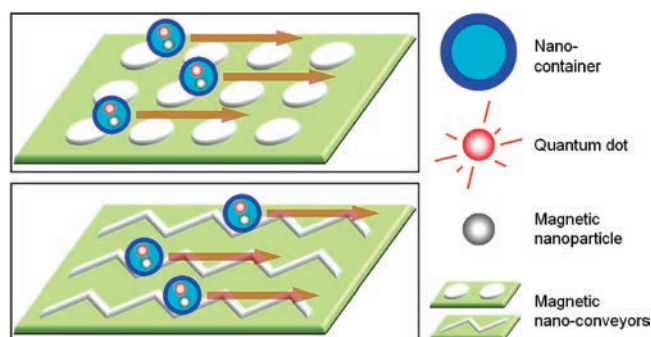


FIGURE 1. Schematic of the nano-conveyor-belt technology. Nano-conveyor-belt arrays can transport multiple individual nanocontainers simultaneously with external control and real-time tracking. Nanocontainers can encapsulate various nanospecies. Here we show encapsulation of quantum dots, which permit long-term tracking with high sensitivity (down to the single nanocontainer level) and magnetic nanoparticles, which permit nanocontainer motion. Nanoconveyors are composed of microfabricated magnetic patterns coupled with electromagnets. The encapsulated magnetic nanoparticles allow nanocontainers to be magnetically manipulated by nanoconveyors.

motion and their controlled manipulation.^{11–15} Conversely, because of their strong fluorescence and resistance to photobleaching, QDs have been used for long-term single particle tracking¹⁴ and optical imaging,¹⁵ demonstrating superiority to traditional fluorescent dyes, which experience photobleaching and photodegradation over time.¹⁶ However, in these technologies QDs play only passive roles. Their positioning and motion cannot be controlled by investigators.^{17–20} The combination of SPIONs and QDs within a nanocontainer provides a mechanism for investigator controlled nanoparticle manipulation with long-term optical tracking capability.

Nanocontainers encapsulating HMQDs (Figure 2a) were formed through interfacial instability.²¹ Amphiphilic block copolymers were initially dissolved in an organic, water-immiscible solvent (e.g., chloroform), and were later dispersed in aqueous solution, yielding water-soluble micelles with hydrophobic cores. QDs and SPIONs with hydrophobic surfaces were incorporated into the hydrophobic cores by addition to the initial, organic phase. The numbers of QDs and SPIONs in each micelle were controlled by the molecular structure of the polymer employed and the quantities of polymer, QDs, and SPIONs used (Supporting Information).

Transmission electron microscopy (TEM) with negative staining (Supporting Information) was used to observe nanocontainer morphology (Figure 2b). QDs and SPIONs (both electron dense) are evident as dark spherical spots within the core of the white, hydrophilic nanocontainer. The diameter of the QD and SPION-filled nanocontainer is ~ 35 nm, substantially smaller than the smallest particles to have been previously magnetically manipulated and simultaneously imaged (i.e., ~ 100 nm).^{13,22} Because SPIONs and QDs (with similar size and shape) cannot be distinguished in TEM, centrifugation in the presence of a magnet was performed to confirm incorporation of both nanoparticles into the nanocontainer. In the presence of a magnet, nanocontainers

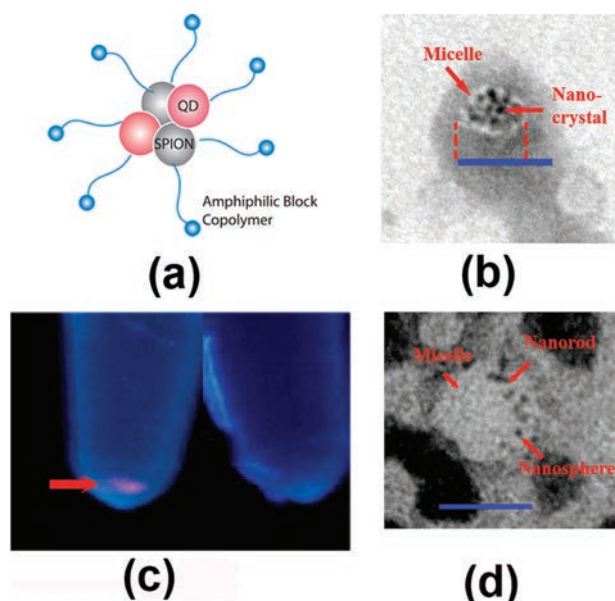


FIGURE 2. Nanocontainers consisting of quantum dots (QDs) and superparamagnetic iron oxide nanoparticles (SPIONs): (a) schematic; (b) TEM with negative staining, scale bar = 50 nm; (c) confirmation of coencapsulation of QDs and SPIONs in nanocontainers. Nanocontainer accumulation (left) in the presence of a magnet and (right) with no magnet. HMQDs fluorescence was observed using a hand-held UV lamp ($\lambda_{em} = 605$ nm); (d) coencapsulation of nanorods and nanospheres, scale bar = 50 nm.

encapsulating HMQDs were attracted to the bottom of a centrifuge tube and could be observed by a hand-held ultraviolet lamp ($\lambda_{em} = 605$ nm) (Figure 2c, left). In contrast, in the absence of a permanent magnet, nanocontainer accumulation was not observed (Figure 2c, right).

Micellar nanocontainers composed of amphiphilic block copolymers are a remarkably versatile encapsulation technology. Multiple individual nanoparticles (>10 , Figure 2b) can be enclosed within the micelle core. In contrast, lipid-PEG micelles⁶ have been reported to encapsulate as little as one nanoparticle.^{6,23} This most likely results from the shorter hydrophobic segment of lipid-PEGs compared to those of amphiphilic block copolymers, which yield a hydrophobic core of only 8 nm vs 20 nm for amphiphilic block copolymers. Also, for lipid-PEG micelles, core size can be dramatically affected by the encapsulated nanospecies. Sailor et al.⁶ reported that adding rod-shaped and spherical nanocrystals to the oil phase created a new lipid-PEG micelle structure several times larger than empty micelles and encapsulating both types of nanocrystals. The larger core appears to be produced as a result of interactions between the lipid-PEG molecules and the nanocrystals enclosed, suggesting that the range of nanomaterials that can be encapsulated with this method is limited. In contrast, block copolymer micelles can theoretically encapsulate any hydrophobic nanomaterial smaller than the micelle core (e.g., carbon nanotubes, gold nanoparticles).²⁴ For example, in addition to the spherical QDs and SPIONs that form the HMQDs studied here, we have also shown coencapsulation

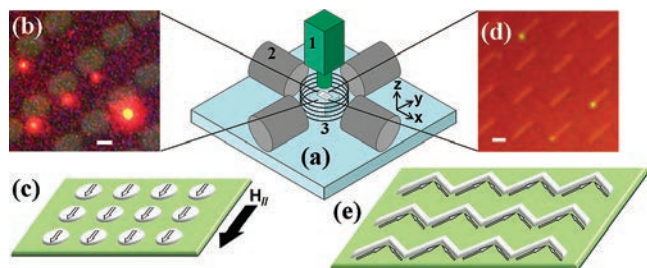


FIGURE 3. (a) Schematic of the magnetic nanoconveyor platform, where label (1) identifies the viewing/tracking microscope, (2) the two pairs of orthogonal miniature tuning electromagnets to create in-plane magnetic fields H_x , H_y , and (3) the coil to create the out-of-plane magnetic field H_z . (b) Superimposed differential interference contrast (DIC)/fluorescence microscopy image of ferromagnetic disks patterned on a silicon substrate and the diffraction limited fluorescent nanocontainers. Scale bar: $2\ \mu\text{m}$. (c) Disk magnetization in the presence of in-plane field H_x , H_y . (d) Superimposed DIC/fluorescence microscopy image of zigzag wires patterned on a silicon surface with three fluorescent nanocontainers trapped at vertices. (e) Direction of magnetization within the zigzag wires after application of a momentary in-plane magnetic field of 1000 Oe. Head-to-head (HH) or tail-to-tail (TT) domain walls are formed at each vertex.

of QD rods and magnetic nanospheres (Figure 2d), demonstrating the broad applicability of this approach.

The second component of the nanoconveyor belt system is the nanoconveyor array technology used for manipulation (Figure 3a). Two distinct conveyor schemes relying on digitized ferromagnetic microdisks (Figure 3b,c) or patterned magnetic nanowires (Figure 3d,e) were developed. The very high field gradients present at the periphery of each disk or at each zigzag vertex are sufficient to trap HMQD nanocontainers as shown in panels b and d in Figure 3. For example, the magnetic field gradient above a magnetic domain wall located at a vertex of a single 380 nm wide, 40 nm thick $\text{Fe}_{0.5}\text{Co}_{0.5}$ zigzag wire (Supporting Information), as used in the present work, is $\sim 3 \times 10^5\ \text{T/m}$ at a height of 40 nm above the platform. Assuming that an average nanocontainer encapsulates ~ 10 SPIONs (Figure 2b) each with a magnetic susceptibility of 1.3,²⁵ this field gradient will generate forces on the order of 0.01 pN to a nanocontainer. As evident from our observations, these forces are sufficient to overcome thermal fluctuations in fluid and trap a single or an aggregate of a few nanocontainer(s). In addition to this feature, the nanoconveyor platform can easily manipulate multiple nanocontainers simultaneously, in contrast to other technologies (i.e., AFM, optical tweezers, and magnetic tweezers).^{3–5}

Synchronizing the directions of the external tuning fields H_x , H_y and the orientation of the weak (<100 Oe) perpendicular H_z field can alter the strength of the trap providing a mechanism for nanocontainer release from traps and their controlled motion in the x – y plane (Supporting Information). For instance, nanocontainers can be moved around the periphery of a disk by rotating the x – y magnetic field, which tracks synchronously with the sharp potential energy minimum (supplementary movie 1 in Supporting Informa-

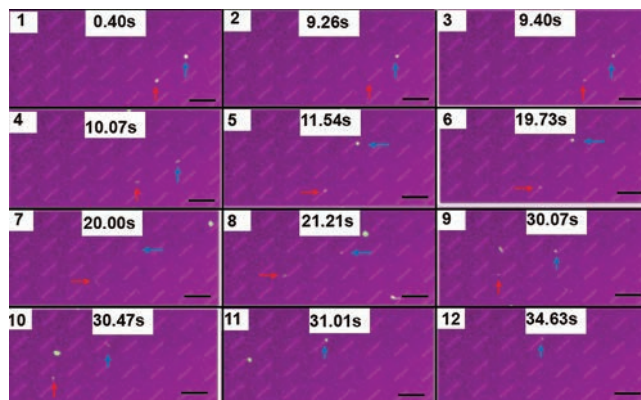


FIGURE 4. Magnetic manipulation and fluorescent tracking of HMQD-filled nanocontainers as shown in selected frames from supplementary movie 3 (Supporting Information) collected using DIC/fluorescence microscopy. Red and blue arrows label individual HMQD-filled nanocontainers that are in flow to the left. The nanocontainers are trapped and released from the platform in response to altering the external magnetic field (H_z) at ~ 10 , 20, and 30 s. Note that at 30 s the H_z change caused the nanocontainer labeled with the red arrow to move out of view. Blinking of encapsulated HMQDs is displayed in frame 2 (red arrow) and frame 10 (blue arrow). Blinking is a probable indicator of single nanocontainers. Scale bar (black) $2\ \mu\text{m}$.

tion). Further, inverting H_z allows nanocontainers to jump to adjacent disks; reversing this sequence returns the nanocontainers to the original disks. By combining rotation with disk-to-disk motion, nanocontainers can be manipulated in investigator-selected directions (supplementary movie 2 in Supporting Information).

Similarly for the wire-based platform, switching the direction of H_z moves nanocontainers between vertices (head-to-head (HH) to tail-to-tail (TT) vertices, or vice versa) permitting migration in the x – y plane. As shown in Figure 4 and supplementary movie 3 (Supporting Information), the platform can also trap and release nanoparticles in a flow stream. While an upward oriented H_z of ~ 100 Oe enhances the field originating from the HH magnetic domain walls, this field weakens trapping forces linked to TT vertices (a downward oriented H_z has the opposite effect). It should be noted that H_z is sufficiently low (<100 Oe) to not affect the structure of magnetic domains. In supplementary movie 3 (Supporting Information), at approximately 10, 20, and 30 s, the direction of H_z was alternated to move HMQD-filled nanocontainers between vertices. Generally, the nanocontainers moved between HH and TT vertices with rare exceptions.

The direction of motion in both the wire and disk systems is determined by the underlying micro-/nanopattern and the investigator-controlled magnetic fields. For example, using the disk system, motion from disk-to-disk can be achieved in virtually any x – y direction; however, for the wire system, motion is confined primarily to a single x – y trajectory, following the pattern of the wires. Additionally, it should be noted that manipulation of each nanoparticle is coordinated;

that is, all particles are moved in the same direction, which can be altered by adjustment of underlying magnetic fields.

The unique fluorescent properties of constituent QDs permitted imaging and tracking of HMQD-filled nanocontainers for at least several hours and confirmation of sub-100-nm size. Because the diameter of a single nanocontainer (~ 35 nm) is smaller than the diffraction limit of optical microscopy (200–300 nm), nanocontainers in fluorescence images appear as solid spherical spots with size determined by the diffraction limit (Figure 4). However, “blinking” exhibited by some nanocontainers (Figure 4, frames (2, 10), and supplementary movie 3 (Supporting Information)) indicates sub-100-nm nanocomposites. Blinking is a characteristic property of single quantum dots, resulting in the intermittent loss of fluorescence signal.²⁰ Because blinking is a stochastic process, small aggregates of quantum dots (i.e., one to four particles) exhibit this behavior,²⁶ whereas in larger aggregates (i.e., greater than four particles), blinking of adjacent QDs is out of phase resulting in a continuous fluorescence signal (supplemental movie 4 in Supporting Information). Using four QDs encapsulated in separate, yet aggregated, nanocontainers as the upper limit for aggregate particle size (an unlikely scenario), the largest blinking nanocomposite composed of fluorescent micelles would be ~ 70 nm (noting the spherical shape of the particle), which is smaller than that of previously imaged 100 nm magnetic nanoparticle composites.¹³ The possibility that fluorescent micelles aggregate with either empty micelles or micelles containing only magnetic nanoparticles, increasing particle size above 100 nm, was also considered; however, using rough probability calculations it can be shown that this is extremely unlikely. All of the blinking, composite nanoparticles observed in this experiment (more than 10) were capable of being manipulated using nanoconveyor arrays. If we assume that the probability of aggregation is $(1/3)$ (based on the experimentally observed ratio of blinking to nonblinking micelles, data not shown), then the probability of all 10 particles consisting of aggregated micelles is $(1/3)^{10}$ or 0.0017%. Even if a larger probability of aggregation is assumed, the probability would need to be $>63\%$ before there is even a 1% chance of all 10 particles manipulated consisting of aggregated micelles. This is extremely unlikely given our experimental observations and the antiadhesive PEG component of the micelles.

We have demonstrated simultaneous magnetic manipulation and fluorescent tracking of sub-100-nm nanocomposites using the nano-conveyor-belt platform, a first step toward externally controlled nanoassembly of multiple particles. This technology is extremely versatile. The disk or wire arrays can be designed and engineered to have different dimensions than those presented here without much effect on trapping ability. Because of their simple design, nanocontainers can encapsulate a wide range of nanomaterials, including quantum dots and rods and magnetic nanoparticles. Apart from the internalized materials, nanocontainer

surfaces could be easily modified with selected chemical moieties or biomolecules through traditional approaches (e.g., using amphiphilic polymers with $-\text{COOH}$ or $-\text{NH}_2$ end groups) for further targeting. The entire nanoconveyor system is small, portable, readily integrated into microfluidic devices, and easily mounted on a reflective fluorescent microscope (Figure 3). Nonspecific binding to the nanoconveyor platform, which could be a significant issue because of the high surface area-to-volume ratio of nanoparticles, is prevented by two unique features of the design. The external surface of the nanocontainers is composed of poly(ethylene glycol) and the nanoconveyers are coated with tri(ethylene glycol). These antiadhesive coatings permit reversible trapping of nanocontainers in the presence of an applied H_z field. Finally, the nanoconveyor array technology is based on patterned magnetic nanowires or disks, whose sizes, shapes, and spacing can be controlled lithographically to create specific device structures. Taken together, this technology allows user control of the materials, nanocontainer surfaces, and conveyor belt design.

Given the versatility of this technology, the nano-conveyor-belt platform could substantially impact a number of fields. For example, in micro-/nanofluidics, sub-100-nm nanostructures could be transported by magnetic manipulation with their individual trajectories being monitored by fluorescence.²⁷ Complex nanostructures could be assembled magnetically with color-coded QDs labeling the individual components.¹ Therapeutic nanoparticles could be magnetically targeted to subcellular locations with nanometer precision, overcoming barriers of intracellular transport.²⁸ Mechanical properties of single biomolecules in the cytoplasm or nucleoplasm of living cells could be probed by examining their force–movement relationships.²⁹

Acknowledgment. Funding of this work is provided by the National Science Foundation (CBET-0707969, EEC-0425626 and CMMI-0900377), the Army Research Office (W911NF-08-1-0455), endowment of the William G. Lowrie family, The Ohio State University Institute for Materials Research (IMR), the Center of Emergent Materials at the Ohio State University an NSF MRSEC (Award Number DMR-0820414), and The Ohio State University. We thank F. Y. Yang and A. J. Hauser for assistance in fabricating the disk and wire arrays.

Supporting Information Available. Details of methods used and captions for supporting videos. This material is available free of charge via the Internet at <http://pubs.acs.org>.

REFERENCES AND NOTES

- (1) Whitesides, G. M.; Grzybowski, B. *Science* **2002**, *295* (5564), 2418–2421.
- (2) Weiss, P. S. *Nature* **2001**, *413* (6856), 585–6.
- (3) Bek, A.; Jansen, R.; Ringler, M.; Mayilo, S.; Klar, T. A.; Feldmann, J. *Nano Lett.* **2008**, *8* (2), 485–490.
- (4) Reck-Peterson, S. L.; Yildiz, A.; Carter, A. P.; Gennerich, A.; Zhang, N.; Vale, R. D. *Cell* **2006**, *126* (2), 335–348.

- (5) Hosu, B. G.; Jakab, K.; Banki, P.; Toth, F. I.; Forgacs, G. *Rev. Sci. Instrum.* **2003**, *74* (9), 4158–4163.
- (6) Park, J. H.; von Maltzahn, G.; Ruoslahti, E.; Bhatia, S. N.; Sailor, M. J. *Angew. Chem., Int. Ed.* **2008**, *47* (38), 7284–7288.
- (7) Vieira, G.; Henighan, T.; Chen, A.; Hauser, A. J.; Yang, F. Y.; Chalmers, J. J.; Sooryakumar, R. *Phys. Rev. Lett.* **2009**, *103*, (12).
- (8) Henighan, T.; Chen, A.; Vieira, G.; Hauser, A. J.; Yang, F. Y.; Chalmers, J. J.; Sooryakumar, R. *Biophys. J.* **2010**, *98* (3), 412–417.
- (9) Wang, N.; Butler, J. P.; Ingber, D. E. *Science* **1993**, *260* (5111), 1124–1127.
- (10) Bausch, A. R.; Moller, W.; Sackmann, E. *Biophys. J.* **1999**, *76* (1), 573–579.
- (11) Dames, P.; Gleich, B.; Flemmer, A.; Hajek, K.; Seidl, N.; Wiekhorst, F.; Eberbeck, D.; Bittmann, I.; Bergemann, C.; Weyh, T.; Trahms, L.; Rosenecker, J.; Rudolph, C. *Nat. Nanotechnol.* **2007**, *2* (8), 495–499.
- (12) Mannix, R. J.; Kumar, S.; Cassiola, F.; Montoya-Zavala, M.; Feinstein, E.; Prentiss, M.; Ingber, D. E. *Nat. Nanotechnol.* **2008**, *3* (1), 36–40.
- (13) Kanger, J. S.; Subramaniam, V.; van Driel, R. *Chromosome Res.* **2008**, *16* (3), 511–22.
- (14) Kaji, N.; Tokeshi, M.; Baba, Y. *Chem. Rec.* **2007**, *7* (5), 295–304.
- (15) Kim, B. Y. S.; Jiang, W.; Oreopoulos, J.; Yip, C. M.; Rutka, J. T.; Chan, W. C. W. *Nano Lett.* **2008**, *8* (11), 3887–3892.
- (16) Chan, W. C.; Nie, S. *Science* **1998**, *281* (5385), 2016–8.
- (17) Adrian, R. J. *Annu. Rev. Fluid Mech.* **1991**, *23*, 261–304.
- (18) Dahan, M.; Levi, S.; Luccardini, C.; Rostaing, P.; Riveau, B.; Triller, A. *Science* **2003**, *302* (5644), 442–445.
- (19) Reese, J.; Chen, R. C.; Fan, L. S. *Exp. Fluids* **1995**, *19* (6), 367–378.
- (20) Saxton, M. J. *Nat. Methods* **2008**, *5* (8), 671–672.
- (21) Zhu, J. T.; Hayward, R. C. *J. Am. Chem. Soc.* **2008**, *130* (23), 7496–7502.
- (22) Tseng, P.; Di Carlo, D.; Judy, J. W. *Nano Lett.* **2009**, *8*, 3053–3059.
- (23) Dubertret, B.; Skourides, P.; Norris, D. J.; Noireaux, V.; Brivanlou, A. H.; Libchaber, A. *Science* **2002**, *298* (5599), 1759–1762.
- (24) Nagarajan, R.; Ganesh, K. *Macromolecules* **1989**, *22* (11), 4312–4325.
- (25) Kim, D. K.; Zhang, Y.; Voit, W.; Rao, K. V.; Muhammed, M. J. *Magn. Magn. Mater.* **2001**, *225* (1–2), 30–36.
- (26) Wang, S.; Querner, C.; Fischbein, M. D.; Willis, L.; Novikov, D. S.; Crouch, C. H.; Drndic, M. *Nano Lett.* **2008**, *8* (11), 4020–4026.
- (27) Lindken, R.; Rossi, M.; Grosse, S.; Westerweel, J. *Lab Chip* **2009**, *9* (17), 2551–2567.
- (28) Whitehead, K. A.; Langer, R.; Anderson, D. G. *Nat. Rev. Drug Discovery* **2009**, *8* (2), 129–138.
- (29) Courty, S.; Luccardini, C.; Bellaiche, Y.; Cappello, G.; Dahan, M. *Nano Lett.* **2006**, *6* (7), 1491–1495.